

Using calorimetric approaches and thermal analysis technology to evaluate critical runaway parameters of azobisisobutyronitrile

Yun-Ting Tsai¹ · Chen-Rui Cao² · Wei-Ting Chen² · Wei-Lung Chou³ · Mei-Li You⁴

Received: 20 November 2014 / Accepted: 13 August 2015 / Published online: 8 September 2015
© Akadémiai Kiadó, Budapest, Hungary 2015

Abstract Azobisisobutyronitrile (AIBN), an azo compound, is widely used in the polymerization reaction process. Due to $-N=N-$ composition of AIBN, it has excellent high thermal sensitivity and decent amounts of decomposition heat. When the cooling system fails, a runaway reaction may occur, leading to a fire or explosion. We used differential scanning calorimetry (DSC) to analyze the thermal hazard parameters of AIBN. Based on DSC thermal data, we can determine the apparent onset temperature (T_0), heat of decomposition (ΔH_d), apparent activation energy (E_a) and its reaction model to evaluate the basic thermal hazard of AIBN. We evaluated the critical runaway parameters of AIBN by Semenov methods, such as critical runaway temperatures and stable temperatures. These critical runaway parameters can be used to describe the unstable reaction criterion, which could determine AIBN's thermal criticality. These results are

able to prevent the thermal hazard and runaway during the production, transportation, and storage of AIBN.

Keywords Azobisisobutyronitrile (AIBN) · Critical runaway temperature (T_c) · Differential scanning calorimetry (DSC) · Runaway reactions · Thermal criticality · Unstable reaction condition

List of symbols

R	Gas constant ($8.31415 \text{ J K}^{-1} \text{ mol}^{-1}$)
A	Pre-exponential factor of Arrhenius equation (min^{-1})
C_0	Original concentration of the material (g cm^{-3})
C	Concentration of the material (g cm^{-3})
C_p	Specific heat of material ($\text{J g}^{-1} \text{ K}^{-1}$)
E_a	Apparent activation energy (kJ mol^{-1})
h	Heat exchange capability index of the cooling system ($\text{kJ m}^{-2} \text{ K}^{-1} \text{ min}^{-1}$)
k	Reaction rate constant (dimensionless)
n	Reaction order (dimensionless)
m	Mass of material (g)
ΔH_d	Heat of decomposition (J g^{-1})
ΔH_t	Heat of decomposition at time (J g^{-1})
ΔH_{total}	Total heat of decomposition (J g^{-1})
$-r$	Reaction rate ($\text{mol L}^{-1} \text{ s}^{-1}$)
q_g	Heat production rate (kJ min^{-1})
q_r	Heat discharge rate (kJ min^{-1})
q_{r1}	Heat discharge rate by high cooling medium (kJ min^{-1})
q_{r2}	Heat discharge rate by cooling system (kJ min^{-1})
q_{r3}	Heat discharge rate by low cooling system (kJ min^{-1})
S	Effective heat exchange area (m^2)
T	Process temperature (K)
T_0	Apparent exothermic temperature (K)

✉ Mei-Li You
mei@ctu.edu.tw

¹ Doctoral Program, Graduate School of Engineering Science and Technology, National Yunlin University of Science and Technology (YunTech), Yunlin, 123, University Rd., Sec. 3, Douliou, Yunlin 64002, Taiwan, ROC

² Department and Graduate School of Safety Health and Environmental Engineering, National Yunlin University of Science and Technology (YunTech), 123, University Rd., Sec. 3, Douliou, Yunlin 64002, Taiwan, ROC

³ Department of Safety, Health, and Environmental Engineering, Hungkuang University, 1018, Taiwan Blvd., Sha-Lu, Taichung 43302, Taiwan, ROC

⁴ Department General Education, Chienkuo Technology University, 32 1, Chiehshou North Rd., Changhua 500, Taiwan, ROC

T_p	Temperature at the maximum heat release in reaction (K)
T_a	Surroundings temperature under cooling system (K)
$T_{a(tr)}$	Surroundings temperature under cooling system at transitional point (K)
T_S	Temperature at the steady state, which occurs at the intersection point of curves q_g and q_r
t	Reaction time (min)
t_p	Transitional point (K)
T_{CI}	Critical ignition or extinction temperature (K)
T_{FCE}	Final critical extinguish temperature (K)
$T_{C(tr)}$	Final critical ignition or extinguish temperature at transitional point (K)
T_{FSE}	Final stable point of extinguish temperature (K)
T_{FSI}	Final stable point of ignition temperature (K)
T_{FSL}	Stable point at low temperatures (K)
T_{FSH}	Stable point at higher temperatures (K)
T_M	Cutoff point between curves q_g and q_r at the highest and lowest cooling efficient system (K)
V	Volume of process instruments (m^3)
X_A	Fractional conversion (dimensionless)
ρ	Density of material ($g\ cm^{-3}$)

Introduction

In chemical reaction processes, there are many occurrences of thermal runaway due to the self-reactive material of azo compounds. Azo compounds are typical self-reactive materials. Owing to the functional group, $-N=N-$, azo compounds are essentially unstable and active. Azobisisobutyronitrile (AIBN), one of the common azo compounds, is focused on various crucial processes contained with the polymerization for common vinyl monomers, blowing agents for the production of vinyl foaming, and some organic reaction processes, and this chemical has been reported as causing many fire and explosion accidents [1].

According to the literature [2], when decomposing, AIBN can release two free nitro radicals at 107 °C, and the decomposition reaction might be terminated immediately by exothermic reaction, which could cause an enormous amount of heat release. AIBN is generally used between 105 and 180 °C in processes. The above-mentioned proved that AIBN processes pose a significant potential hazard. Unfortunately, the critical runaway of AIBN reveals that temperatures and unstable criteria of AIBN are still unknown to date.

In general, as the heat production rate exceeds the rate of heat removed, heat can be accumulated in the reaction system to cause temperature to be increased. When the system temperature reaches the apparent exothermic onset

temperature (T_0), this reaction system gradually becomes unstable and a self-reactive reaction is activated. As the temperature attains a specific threshold value, this reactive system will inevitably trigger a runaway reaction or even explosion [3–6].

A literature review was conducted to determine thermal runaway reaction of AIBN by using differential scanning calorimetry (DSC) under various heating rates (β). The reaction kinetics prediction model was employed to evaluate reaction kinetics, apparent exothermic temperature (T_0), reaction order (n), temperature at the maximum heat release in reaction (T_p), heat of decomposition (ΔH_d), pre-exponential factor (A), and apparent activation energy (E_a). Above-mentioned thermokinetic parameters of AIBN were used to determine the critical runaway temperatures and stability criterion of AIBN's reaction. The calculated kinetic parameters and measured exothermic reaction heat were substituted into the various critical parameters by the formula of thermal explosion [7] to define the critical runaway reaction. The required heat transfer coefficients (hS) in this critical condition could also be estimated.

Experimental and methods

Thermokinetic parameters of AIBN reaction

The reaction thermokinetic parameters of 98 mass% AIBN were determined by Li et al. [8] (see Tables 1, 2).

To calculate the critical conditions in this exothermic reaction of AIBN, thermal hazard parameters of AIBN reaction must be defined, such that E_a and A could be used to acquire thermal hazard information using reliable kinetic and Ozawa models. We can compute the thermokinetic parameters through the following equation from Kissinger and Ozawa models, as Eqs. (1) and (2), respectively [9–11]:

$$\ln\left(\frac{\beta}{T_p^2}\right) = \ln\left(\frac{AR}{E_a}\right) - \frac{E_a}{RT_p} \quad (1)$$

$$\ln(\beta) = -1.0516 \frac{E_a}{RT_p} + C \quad (2)$$

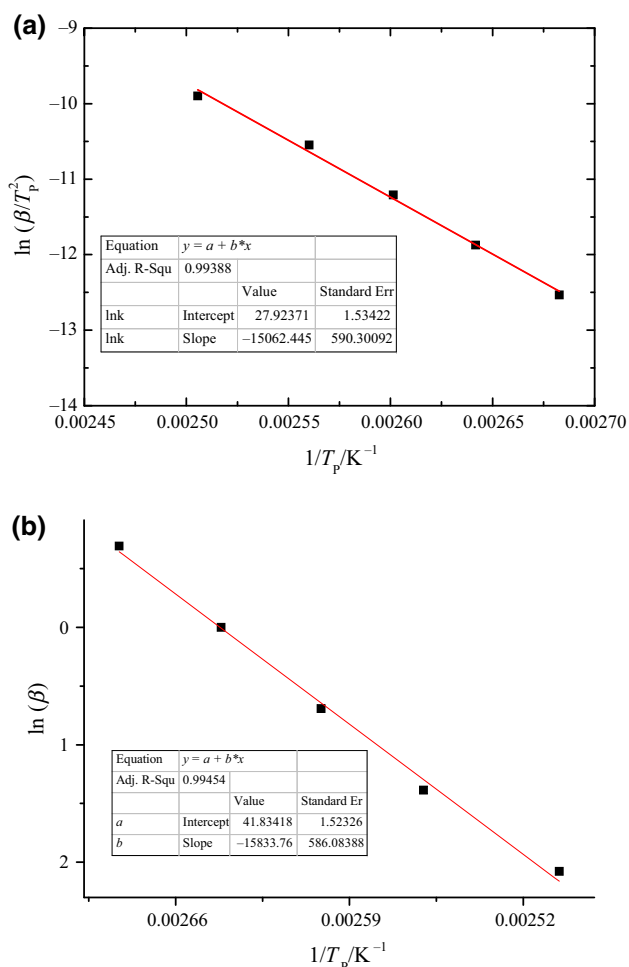
Table 1 Non-isothermal data by DSC tests for 98 mass% AIBN at 0.5, 2.0, 2.5, 5.0, and 10.0 °C min⁻¹

$\beta/^\circ\text{C min}^{-1}$	$T_0/^\circ\text{C}$	$T_p/^\circ\text{C}$	$\Delta H_d/\text{J g}^{-1}$
0.5	93.0	99.8	875.0
2.0	101.0	105.5	837.0
2.5	107.0	111.4	887.0
5.0	113.0	117.6	1097.0
10.0	121.0	126.1	1185.0

Table 2 Critical conditions for 98 mass% AIBN

T_c/K	T_s/K	$hS/kJ\ min^{-1}\ K$
441.06 (ex.)	304.65 (Low)	3.495
305.25 (ig.)	558.73 (High)	0.018

The kinetic parameters A and E_a can be determined by plotting the values of $\ln[\beta/T_p^2]$ against $1/T_p$ via Kissinger method. In addition, we also employed the Ozawa method to determine E_a by plotting the values of $\ln[\beta]$ against $1/T_p$ and compared the results from Kissinger method [12–14]. The evaluated thermokinetic parameters for the AIBN reaction by Kissinger and Ozawa method are shown in Fig. 1. We observed a large degree of similarity between E_a values derived from simulation results of two methods with the values of ca. 125.0 and 124.0 kJ mol⁻¹, respectively. Therefore, the calculation results could be used as reliable information for our study.

**Fig. 1** Evaluation of E_a by (a) Kissinger method and (b) Ozawa method for 98 mass% AIBN at $n = 1.0$

Stability principles and critical runaway parameters for AIBN's reaction

Reaction concentration can be converted to Eqs. (3) and (4) [15–18]:

$$X_A = \frac{\Delta H_t}{\Delta H_{\text{total}}} = \frac{[mC_p(T - T_o)]}{[mC_p(T_p - T_o)]} = \frac{(T - T_o)}{(T_p - T_o)} \quad (3)$$

$$C = C_o(1 - X_A) = C_o(T_p - T)/(T_p - T_o) = C_o(T_p - T)/\Delta T_p \quad (4)$$

where C is the concentration of the material, C_o is the original concentration of the material, X_A is the fractional conversion, ΔH_t is the heat of decomposition at time, ΔH_{total} is the total heat of decomposition, m is the mass of material, and C_p is the specific heat of material.

The reaction rate (r) equation can be represented as Eq. (5):

$$-r = -dC/dt = kC^n \quad (5)$$

where k is the reaction rate constant, t is the reaction time, and n is the reaction order.

Substituting and conjoining Eq. (4) into Eq. (5) with the Arrhenius equation:

$$k = C_o^{n-1}A \exp(-E_a/RT) = (dT/dt)/[(T_p - T)/\Delta T_p]^n \Delta T_p \quad (6)$$

Taking the natural logarithms on equation renders the following:

$$\ln k = \ln \left\{ (dT/dt)/[(T_p - T)/\Delta T_p]^n \Delta T_p \right\} = \ln(C_o^{n-1}A) - E_a/RT \quad (7)$$

Temperature rise rate can be represented as dT/dt by adiabatic measurement mode.

Semenov model indicates that heat production rate (q_g) can be expressed by the following parameters: volume of reactant (V), $-r$, and ΔH_{total} . q_g is represented as Eq. (8) [19–21]:

$$q_g = \Delta H_{\text{total}}V(-r) \quad (8)$$

Replacing Eq. (5) into Eq. (8), q_g can be rewritten as Eq. (9):

$$q_g = \Delta H_{\text{total}}VAC^n \exp(-E_a/RT) \quad (9)$$

The heat discharge rate (q_r) from the process equipment to the cooling system or cooling medium is denoted as Eq. (10):

$$q_r = hS(T - T_a) \quad (10)$$

where h is the heat exchange capability index of the cooling system, S is the effective heat exchange area, and T_a is the surroundings temperature under cooling system.

The energy equilibrium in the reaction can be expressed as Eq. (9) subtracting Eq. (10) and finishing as Eq. (11):

$$\rho VC_p(dT/dt) = q_g - q_r \quad (11)$$

where ρ is the density of material.

From Eq. (9) to Eq. (11), the energy balance in the reaction can be expressed as Eq. (12):

$$\rho VC_p(dT/dt) = \Delta H_{\text{total}} VAC^n \exp((-E_a/RT)) - hS(T - T_a) \quad (12)$$

As described above, in the computations of thermokinetic parameters of AIBN, we assume that n is a first-order reaction. Thus, replacing Eq. (9) into Eq. (12) with $n = 1$, Eq. (12) can be rephrased as Eq. (13):

$$\rho VC_p(dT/dt) = \Delta H_{\text{total}} VAC_o [(T_p - T)/(T_p - T_o)] \exp((-E_a/RT)) - hS(T - T_a) \quad (13)$$

At steady state, Semenov's reaction state discriminant equations for a "critical situation of the reaction system" can be annotated as Eqs. (14) and (15) [22, 23]:

$$q_g|_{T=T_c} = q_r|_{T=T_c} \quad (14)$$

$$\left. \frac{dq_g}{dT} \right|_{T=T_c} = \left. \frac{dq_r}{dT} \right|_{T=T_c} \quad (15)$$

where T_c is the critical temperature.

When the range of q_g and q_r is negative, $(dT/dt) > 0$. Heat gathering exceeds the handling capacity of the cooling system. Eventually, the system will produce a thermal runaway reaction. Equation (13) can be rewritten as Eq. (16):

$$\Delta H_{\text{total}} VAC_o [(T_p - T_c)/(T_p - T_o)] \exp((-E_a/RT_c)) = hS(T_c - T_a) \quad (16)$$

Applying the conditions of Eqs. (14) and (15) gives:

$$hS = \frac{\Delta H_{\text{total}} VAC_o \exp((-E_a/RT_c)) [-1 + E_a(T_p - T_c)/RT_c^2]}{(T_p - T_o)} \quad (17)$$

After dividing Eq. (16) by Eq. (17), the T_c can be obtained by Eq. (18):

$$\frac{E_a}{RT_c^2} = \frac{1}{(T_c - T_a)} + \frac{1}{(T_p - T_c)} \quad (18)$$

T_c can be explained as Eq. (18) [24, 25]:

$$T_c = \frac{(T_p + T_a) \pm \sqrt{(T_p + T_a)^2 - 4[1 + R(T_p - T_a)/E_a] T_p T_a}}{2[1 + R(T_p - T_a)/E_a]} \quad (19)$$

Results and discussion

According to Eqs. (14) and (15), Semenov defined the critical conditions of a reaction system; from the above definitions, the critical conditions are not barely the intersection point of trajectory formed by q_g and q_r ; the critical conditions also contain the tangent point of heat production rate curves and heat removal rate curve. These parameters are critical ignition or extinction temperature (T_{CI}) and final stable point of ignition temperature (T_{FSI}) at low performance of cooling treatment, final stable point of extinguish temperature (T_{FSE}), and final critical extinguish temperature (T_{FCE}) at high performance of cooling treatment, stable point at low temperatures (T_{FSL}) and stable point at higher temperatures (T_{FSH}) at medium performance of cooling treatment.

The space containing critical conditions could be applied to decide the stability region of the AIBN reaction system. T_a can be substituted into arbitrary value; we chose ambient temperature as 300 K in Figs. 2, 3, 4, 5, 6 and 7. These six figures show the balance of the q_g and q_r versus the T_a . From Eq. (19), the two solutions, T_{FCE} and T_{CI} , can be therefore acquired, and then, the two critical temperatures can be taken into Eq. (17) to obtain two different hS values. These two parameters with Eq. (19) can be used to decide the other critical conditions.

Low performance of cooling treatment

Figures 2 and 3 show the heat balance between the q_g and q_r in low performance of cooling treatment. As the

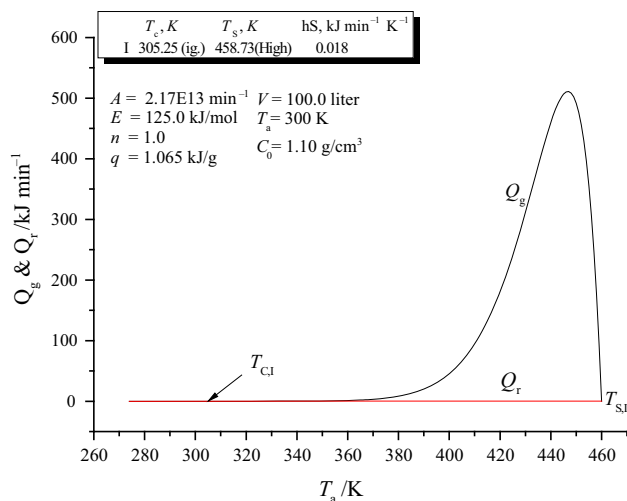


Fig. 2 Balance diagram of heat production rate q_g and low heat removal rate q_r for decomposition reaction of 98 mass% AIBN

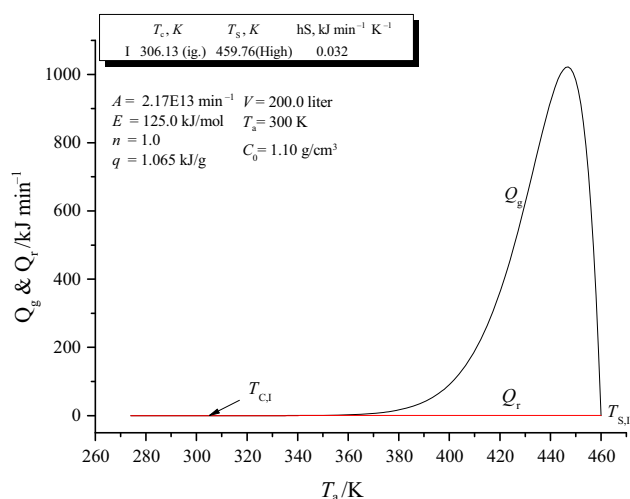


Fig. 3 Balance diagram of heat production rate q_g and low heat removal rate q_r for decomposition reaction of 98 mass% AIBN with reactor volume = 200.0 L

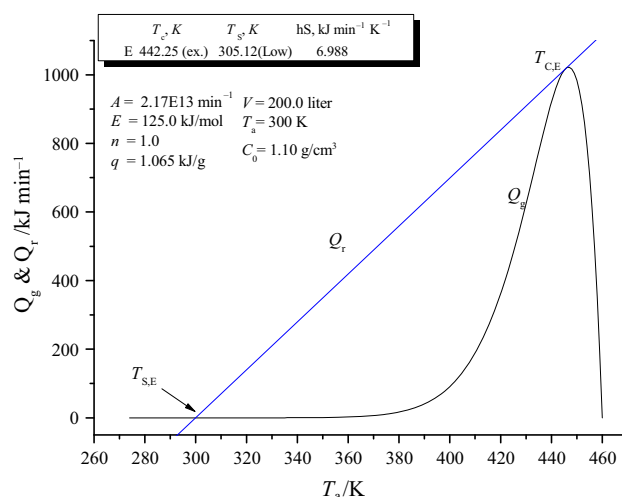


Fig. 5 Balance diagram of heat production rate q_g and high heat removal rate q_r for decomposition reaction of 98 mass% AIBN with reactor volume = 200.0 L

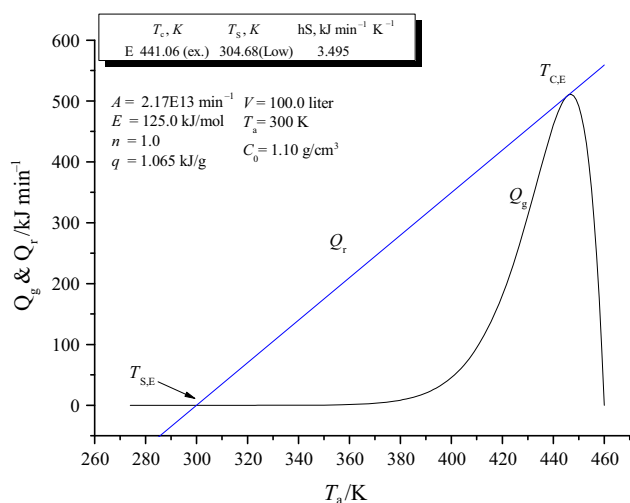


Fig. 4 Balance diagram of heat production rate q_g and high heat removal rate q_r for decomposition reaction of 98 mass% AIBN

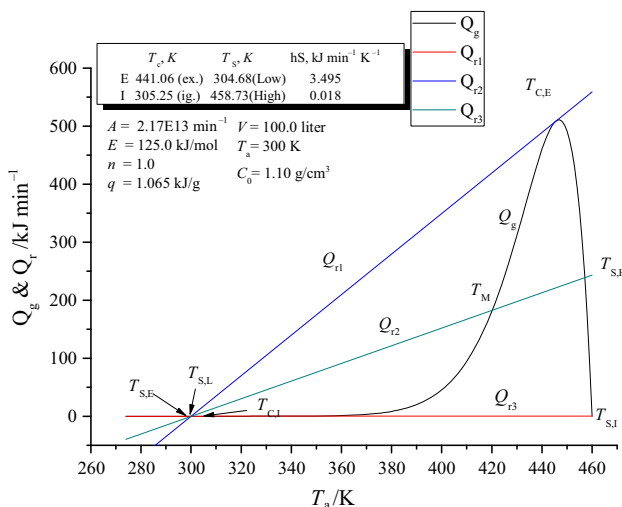


Fig. 6 Balance diagram of heat production rate q_g and heat removal rate q_r for decomposition reaction of 98 mass% AIBN

temperature T in the reaction system of AIBN at steady state was less than T_{FCI} , at this time, q_g was greater than q_r , generated heat accumulation in the reaction system, resulted in a temperature rise, and headed for point T_{FSI} . Finally, T reached T_{FSI} and would eventually exceed this point. The opposite situation, q_{r1} , was greater than q_g . Consequently, the value of T increased and moved back to point T_{FSI} . Points of T_{FSI} were the final stable point of ignition temperature. These points could be expressed as the temperature of reaction that never ascended and never declined at $hS = 0.018 \text{ kJ min}^{-1} \text{ K}^{-1}$.

High performance of cooling treatment

Figures 4 and 5 show the heat balance between the heat production rate q_g and the heat production rate q_r in high performance of cooling treatment. The intersection point and tangent point of q_g and q_{r3} curves were T_{FSE} and T_{FCE} . When the T was less than T_{FSE} , q_{r3} was less than q_g ; T increased and recovered to T_{FSE} . When the T was higher than T_{FSE} , q_{r3} was greater than q_g . T dropped to T_{FSE} back again. When the T was greater than T_{FCE} , q_{r3} was higher than the q_g , T moving back to point T_{FCE} . These two points are also described as the temperature that never decreased, and the

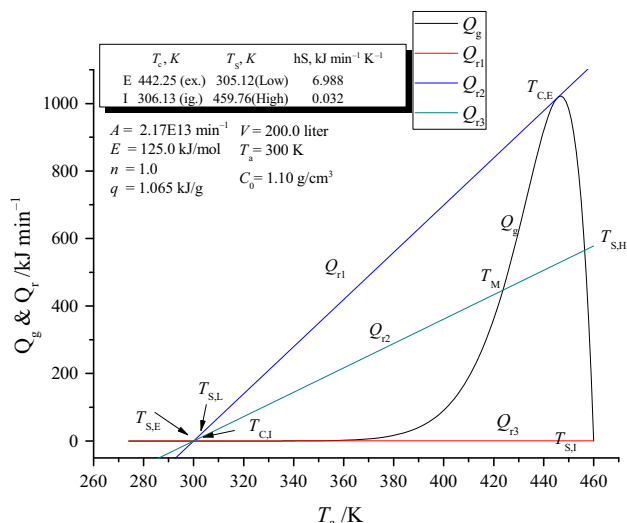


Fig. 7 Balance diagram of heat production rate q_g and heat removal rate q_r for decomposition reaction of 98 mass% AIBN with reactor volume = 200.0 L

temperature of no return at $hS = 3.495$ and $6.988 \text{ kJ min}^{-1} \text{ K}^{-1}$ at reactor volume was 100 and 200 L, respectively.

Medium performance of cooling treatment and heat transfer coefficients (hS)

Figures 6 and 7 delineate the heat balance between the heat production rate q_g and the heat discharge rate q_r in medium performance of cooling treatment. When the range of hS was in $0.032 < hS < 6.988$ and $0.000039 < hS < 532.323 \text{ kJ min}^{-1} \text{ K}^{-1}$, reactor volume was 100 and 200 L, respectively. There were three intersection points including T_{FSL} , T_M , and T_{FSH} at trajectory of q_{r2} and q_g . In particular, T_M means that cutoff point between curves q_g and q_r was at the highest and lowest cooling efficient systems.

Trajectory of q_{r2} is shown as a dotted line. On former analysis, it was difficult to maintain an equilibrium state at $T = T_M$ owing to the variability of this temperature. We supposed that the reaction system began accurately at the T_M ; as long as the process parameters of any minor alternations would deviate the reaction system from the stable state, they would no longer return to T_M but cause T rise or fall to the T_{FSL} or T_{FSH} in a steady state, respectively. Thus, a tiny upsurge in T would encourage q_g growth and accelerated the T even higher. In contrast to the situation of the T increase, the minor temperature drop would make the q_r greater than q_g , which would cause the T to decline again. The medium steady temperature T_M was erratic and sensitive. In contrast, T_{FSL} and T_{FSH} would be stable; if the disturbance occurs in any way, reaction would reoccur to

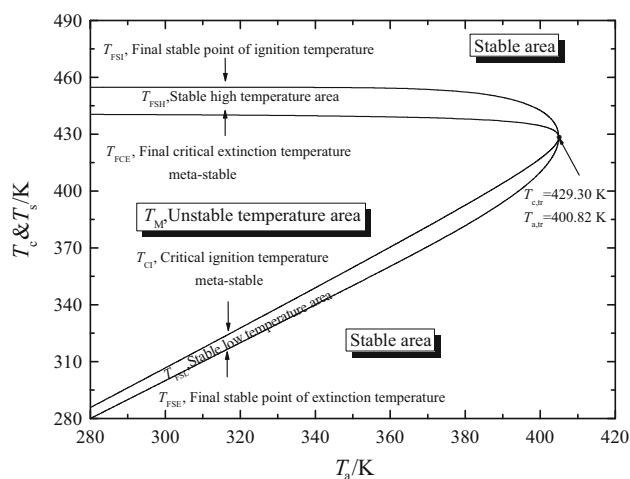


Fig. 8 Correlation of evaluated temperatures T_{CI} , T_{FCE} , T_{FSI} , and T_{FSE} versus ambient temperature T_a for decomposition reaction of 98 mass% AIBN

unstable state. Table 2 lists critical conditions for 98 mass% AIBN.

Transition point phenomenon

Figure 8 depicts the critical conditions of T_{CI} , T_{FCE} , T_{FSI} , and T_{FSE} against T_a by using the above equations for the decomposition reactions of AIBN. These parameters have the following behavior: $T_{FSI} > T_{FCE} > T_{CI} > T_{FSE}$. Both T_{FSI} and T_{FCE} alleviated, and both T_{FCI} and T_{FSE} heightened progressively with increasing T_a . T_a rises to a specific value of the transitional point of T_a (tr); all of the critical conditions would eventually intersect at a transitional point, T_c (tr). The T_a (tr) could be inferred from Eqs. (20) and (21):

$$T_{a(tr)} = \frac{1}{(E_a + 4RT_p)} \quad (20)$$

$$T_{c(tr)} = \frac{1}{(E_a + 2RT_p)} \quad (21)$$

Even as $q_g < q_r$ in reaction, it is still not enough to express the reaction system as stable. Reaction state also must satisfy the following conditions:

$$\text{If } T - T_s > 0, \quad q_g < q_r$$

or

$$\text{If } T - T_s < 0, \quad q_g > q_r \quad (22)$$

Here T_s is defined as a stable temperature in a reaction system at the state of $q_g = q_r$. Equation (22) indicates that these two discriminant functions are necessary and sufficient conditions for determining and deciding the stability

of the reaction. The stable conditions have been predicted and estimated by Lu et al. [24, 25].

By the aforementioned conditions and equations, the stable criteria of AIBN could be decisive. If the T surpassed over the trajectory for T_{FSI} or under the trajectory for T_{FSE} , the system was stable. T would eventually return to these two temperatures. When the T was interposed between the trajectory for T_{FCI} and T_{FCE} , the system was unstable. Additionally, the following range of parameters formed two stable areas: $T_{FSE} < T_{FSL} < T_{CI}$ and $T_{FCE} < T_{FSH} < T_{FSI}$. As the T_a was augmented, T_{FSI} and T_{FCE} temperature trajectories were reduced, where the T_{CI} and T_{FSE} temperature trajectories were expanded and augmented at the same time. These four temperature trajectories moved increasingly. At the time that T_a surpassed 400.82 K, these temperature trajectories clustered gathered at the $T_{c(tr)}$ and the value of the $T_{c(tr)}$ was 429.30 K.

Conclusions

After assessing the thermokinetic data, we could mimic the scale-up situation and avoid arriving at the critical temperature. The results are shown in Figs. 2–8. In high performance cooling treatment medium, the critical temperature in high temperature and low temperature was 441.06 and 305.25.15 K, respectively. Through individual low performance cooling treatment medium, the critical temperature in high temperature and low temperature was 458.73 and 304.68 K, respectively. The unstable temperature area was enclosed by the trajectories T_{CI}/T_{FSI} at high performance and T_{FCE}/T_{FSE} in low performance. In exclusion of unstable region, the reaction system of AIBN was stable.

In this study, the reaction and thermal hazard could be effectively evaluated by simulation of required heat removal rate for cooling system during the chemical process. In the future, isothermal kinetic model could be obtained by isothermal calorimeter, TAM III, to calculate *SADT* or other safety parameters by Semenov model as control temperature for AIBN during transportation and storage.

References

- Liu SH, Yu YP, Lin YC, Weng SY, Hsieh TF, Hou HY. Complex thermal evaluation for 2, 20-azobis (isobutyronitrile) by non-isothermal and isothermal kinetic analysis methods. *J Therm Anal Calorim.* 2013;112:1361–7.
- Roduit B, Hartmann M, Folly P, Sarbach A, Brodard P, Baltenasperger R. Determination of thermal hazard from DSC measurements. Investigation of self-accelerating decomposition temperature (*SADT*) of AIBN. *J Therm Anal Calorim.* 2014;117:1017–26.
- Lin CP, Tseng JM, Chang YM, Liu SH, Cheng YC, Shu CM. Modeling liquid thermal explosion reactor containing tert-butyl peroxybenzoate. *J Therm Anal Calorim.* 2010;102:587–9.
- You ML, Tseng JM, Liu MY, Shu CM. Runaway reaction of lauroyl peroxide with nitric acid by DSC. *J Therm Anal Calorim.* 2010;102:535–9.
- Luo KM, Chang JG, Lin SH, Chang CT, Yeh TF, Hu KH, Kao CS. The criterion of critical runaway and stable temperatures in cumene hydroperoxide reaction. *J Loss Prev Process Ind.* 2001;14:229–39.
- Tsai YT, You ML, Qian XM, Shu CM. Calorimetric techniques combined with various thermokinetic models to evaluate incompatible hazard of tert-butyl peroxy-2-ethyl hexanoate mixed with metal ions. *Ind Eng Chem Res.* 2013;52:8206–15.
- Lu KT, Luo KM, Lin PC, Hwang KL. Critical runaway conditions and stability criterion of RDX manufacture in continuous stirred tank reactor. *J Loss Prev Process Ind.* 2005;18:1–11.
- Li XR, Wang XL, Koseki H. Study on thermal decomposition characteristics of AIBN. *J Hazard Mater.* 2008;159:13–8.
- Boswell PG. On the calculation of activation energies using a modified Kissinger method. *J Therm Anal Calorim.* 1980;18:353–8.
- Marco E, Cuartielles S, Peña JA, Santamaria J. Simulation of the decomposition of di-cumyl peroxide in an ARSST unit. *Thermochim Acta.* 2002;362:49–58.
- Snee TJ, Barcons C, Hernandez H, Zaldivar JM. Characterisation of an exothermic reaction using adiabatic and isothermal calorimetry. *J Therm Anal Calorim.* 1992;38:2729–47.
- Li XR, Koseki H. *SADT* prediction of autocatalytic material using isothermal calorimetry analysis. *Thermochim Acta.* 2005;431:113–6.
- Carmona VB, Oliveira RM, Silva WTL, Mattoso LHC, Marconcini JM. Nanosilica from rice husk: extraction and characterization. *Ind Crop Prod.* 2013;43:291–6.
- Bartknecht W. Explosions: course, prevention, and protection. New York: Springer; 1981.
- Semenov NN. Thermal theory of combustion and explosion. *Usp Fiz Nauk.* 1940;23:4–17.
- Semenov NN. Zur theorie des verbrennungsprozesses. *Z Phys Chem.* 1928;48:571–3.
- Morbidelli M, Varma A. A generalized criterion for parametric sensitivity: application to thermal explosion theory. *Chem Eng Sci.* 1988;43:91–8.
- Wu SH. Runaway reaction and thermal explosion evaluation of cumene hydroperoxide (CHP) in the oxidation process. *Thermochim Acta.* 2013;559:92–7.
- Eigenberger G, Schuler H. Reactor stability and safe reaction engineering. *Int Chem Eng.* 1989;29:12–9.
- Villiermaux J, Georgakis C. Current problems concerning batch reactions. *Int Chem Eng.* 1991;31:434–41.
- Lee RY, Hou HY, Tseng JM, Chang MK, Shu CM. Reaction hazard analysis for the thermal decomposition of cumene hydroperoxide in the presence of sodium hydroxide. *J Therm Anal Calorim.* 2008;93:269–70.
- Wu KW, Hou HY, Shu CM. Thermal phenomena studies for dicumyl peroxide at various concentrations by DSC. *J Therm Anal Calorim.* 2006;83:41–4.
- Kohlbrand HT. The use of SimuSolv in the modeling of ARC (accelerating rate calorimeter) data, International symposium on runaway reactions. New York: AIChE; 1989. p. 86–111.
- Lu KT, Yang CC, Lin PC. The criteria of critical runaway and stable temperatures of catalytic decomposition of hydrogen peroxide in the presence of hydrochloric acid. *J Hazard Mater.* 2006;135:319–27.
- Lu KT, Luo KM, Lin SH, Su SH, Hu KH. The acid-catalyzed phenol-formaldehyde reaction: critical runaway conditions and stability criterion. *Process Saf Environ Prot.* 2004;82:37–47.